

A Compromise Principle in Deep Monocular Depth Estimation

Huan Fu, Mingming Gong, Chaohui Wang, and Dacheng Tao, *Fellow, IEEE*

Abstract—Monocular depth estimation, which plays a key role in understanding 3D scene geometry, is fundamentally an ill-posed problem. Existing methods based on deep convolutional neural networks (DCNNs) have examined this problem by learning convolutional networks to estimate continuous depth maps from monocular images. However, we find that training a network to predict a high spatial resolution continuous depth map often suffers from poor local solutions. In this paper, we hypothesize that achieving a compromise between spatial and depth resolutions can improve network training. Based on this “compromise principle”, we propose a regression-classification cascaded network (RCCN), which consists of a regression branch predicting a low spatial resolution continuous depth map and a classification branch predicting a high spatial resolution discrete depth map. The two branches form a cascaded structure allowing the main classification branch to benefit from the auxiliary regression branch. By leveraging large-scale raw training datasets and some data augmentation strategies, our network achieves competitive or state-of-the-art results on three challenging benchmarks, including NYU Depth V2 [1], KITTI [2], and Make3D [3].

Index Terms—Depth Prediction, Depth Resolution, Spatial Resolution, Compromise Principle, SID, Convolutional Neural Network

I. INTRODUCTION

ESTIMATING depth from 2D images is a key component of scene reconstruction and understanding tasks, such as 3D recognition, tracking, segmentation and detection [4], [5], [6], [7], [3], [8], [9], [10], [11], [12], *etc.* In this paper, we examine the problem of *Monocular Depth Estimation* (abbr. as *MDE* hereafter), namely the estimation of the depth map from a single image.

Compared to depth estimation from stereo images or video sequences, in which significant progress has been made [13], [14], [15], [16], [10], [17], [18], [19], progress in MDE has been slow. MDE is fundamentally an ill-posed problem: a single 2D image may be produced from an infinite number of distinct 3D scenes. Fortunately, the 2D image and the depth map are correlated, suggesting that the depth can still be predicted with considerable accuracy.

To overcome this inherent ambiguity, typical methods resort to exploiting statistically meaningful monocular cues or

features, such as perspective and texture information, object sizes, object locations, and occlusions. Previous methods used handcrafted features for depth estimation [3], [20], [21], [22], [23], [24], [25], [26], [27], [28], [29], but since the handcrafted features alone can only capture local information, probabilistic graphic models [30], [3] or depth transfer methods [18] have been introduced to incorporate long range global cues.

Buoyed by the success of deep convolutional neural networks (DCNNs) in object recognition and detection, several recent works have significantly improved the MDE performance by a large margin with the use of DCNN-based models [31], [32], [33], [34], [35], [36], demonstrating that deep features are superior to handcrafted features. The main advantage of DCNNs is that the hierarchical representations in a DCNN capture both local and global information. A state-of-the-art method [34] exploits the multi-scale network which firstly learns to predict a coarse depth map using global information and then refines it using another network with local information to produce a fine depth map.

Existing methods address the MDE problem by learning a CNN to estimate the continuous depth map. Since this problem is a standard regression problem, existing methods usually adopt the root mean squared error (RMSE) in log-space as the loss function. Although training with RMSE can achieve a reasonable solution when predicting a low resolution depth map, we find that the optimization tends to be difficult when we try to train networks to predict high-resolution continuous maps. The stochastic gradient descent (SGD) optimization method usually produces a local solution with unsatisfactory training error in this case.

We hypothesize that a compromise between spatial and depth resolution can make the optimization easier, which is referred to as the “compromise principle” in this paper. According to the compromise principle, we avoid directly estimating a high spatial resolution continuous depth map by firstly estimating depth maps with reduced spatial or depth resolution. To reduce the depth resolution, we propose to transform the regression problem into a classification problem by discretizing the depth value into intervals. Employing the classification loss to train the network achieves lower RMSE on the training data than training with RMSE. Also, the low spatial resolution continuous map can be learned with considerable accuracy. Based on such a principle, we develop a regression-classification cascade network (RCCN) which consists of two branches: 1) the regression branch predicting low spatial resolution continuous depth map from the fully-connected layers, capable of capturing global scene information; and 2) the classification branch, which predicts high

H. Fu and D. Tao are with UBTECH Sydney AI Centre, SIT, FEIT, The University of Sydney, J12 Cleveland St, Darlington NSW 2008, Australia (e-mail: hufu6371@uni.sydney.edu.au; dacheng.tao@sydney.edu.au).

M. Gong is with Department of Biomedical Informatics, University of Pittsburgh, Cubicle 520c, 5607 Baum Bouevard, Pittsburgh, PA 15206 (e-mail: minggongnju@gmail.com).

C. Wang is with Laboratoire d'Informatique Gaspard Monge - CNRS UMR 8049, Université Paris-Est, 77454 Marne-la-Vallée Cedex 2, France (e-mail: chaohui.wang@u-pem.fr).

spatial resolution discrete depth maps from the convolutional layers to preserve finer spatial information. The two branches form a cascaded structure and are learned jointly in an end-to-end fashion, which allows the classification and regression branches to benefit from each other. After accomplishing the RCCN learning stage, a refinement and a fusion networks are posted to refine the discrete depth map into a higher spatial resolution. Our network achieves competitive or state-of-the-art performance on NYU Depth V2 [1], KITTI [2], and Make3D [30], [3] benchmarks, which are three challenging datasets commonly used for MDE.

II. RELATED WORK

Depth estimation is an important part of understanding the 3D structure of scenes from 2D images. Most prior works focused on estimating depth from stereo images by developing geometry-based algorithms [37], [38] that rely on point correspondences between images and triangulation to estimate the depth. Given accurate point correspondences, depth can be estimated deterministically from stereo images. Thus, stereo depth estimation has particularly benefitted largely from the advances in local feature matching and dense optical flow estimation techniques.

However, the geometry-based depth estimation algorithms for stereo images ignore the monocular cues in 2D images, which can also be used for depth estimation. In a seminal work [30], Saxena *et al.* learned the depth from monocular cues in 2D images via supervised learning. Since then, a variety of approaches have been proposed to exploit the monocular cues using handcrafted representations [3], [20], [21]. Since handcrafted features alone can only capture local information, probabilistic graphic models such as Markov Random Fields (MRFs) are often built on these features to incorporate long-range and global cues [3], [39], [40]. Another successful way to make use of global cues is the DepthTransfer method [18] which uses GIST global scene features [41] to search for candidate images that are “similar” to the input image from a database containing RGBD images. A warping procedure based on SIFT Flow [42] was then applied to the candidate image and the corresponding depth map to align them to the input image.

Given the success of DCNNs in image understanding [43], [44], [45], [46], some DCNNs based depth prediction frameworks have recently been proposed in recent years [47], [32], [48], [36]. Xie *et al.* [49] predicted the disparity map by adopting multi-level convolutional features for recovering a right view from a left-view. Garg *et al.* [47] proposed an unsupervised framework to learn a deep depth-estimation neural network. Liu *et al.* [31] jointly explored the capacity of DCNNs and continuous CRF in a unified deep structured network. Moreover, Wang *et al.* [32] captured depth values and semantic information in a scene with DCNNs, and integrated them in a two-layer hierarchical CRF to jointly predict depth values and semantic labels. To improve efficiency, Roy and Todorovic [33] proposed the Neural Regression Forest method which allowed for parallelisable training of “shallow” CNNs. To further incorporate global information in DCNNs, Wang

et al. [50] proposed a method for surface normal prediction, where two independent networks were learned to exploit global and local information respectively. Eigen *et al.* [51], [34] proposed a multi-scale network that firstly learned to predict depth at a coarse scale and then refined it using another network to produce fine-scale depth maps. Further, Iro *et al.* [52] suggested to adopt deeper network to learn better image representations towards depth estimation.

Most recently, considering limited labeled samples and expensive human resources, some impressive unsupervised and semi-supervised [47], [49], [48], [36], [53], [54] methods were developed by posing monocular depth estimation as an image reconstruction problem. For example, Xie *et al.* [49], Garg *et al.* [47] and Godard *et al.* [48] address the problem of novel view synthesis, and design reconstruction losses to estimate the disparity map by recovering a right view from a left view. In further, Kuznetsov *et al.* [36] incorporated extra supervision via ground truth depth in aforementioned unsupervised frameworks to improve the training. Also, Zoran *et al.* [53] and Chen *et al.* [54] optimized depth estimation networks from selected patch pairs from images via pair-wise ranking losses, where the ordinal annotation a pair (A, B) is only d_A closer to d_B , d_A further to d_B and d_A equal to d_B .

Our RCCN method also explores global and local representations in the network for depth prediction in a supervised manner. However, our network architecture is motivated by exploiting the compromise between spatial and depth resolutions. Thus, instead of designing a stage-wise refinement procedure as done in [51], we introduce a cascaded structure to learn low spatial resolution but high depth resolution continuous depth via regression and high spatial resolution but low depth resolution discrete depth via classification in an end-to-end fashion. In addition, to exploit large receptive field and to alleviate information loss caused by downsampling operation, we introduce dilated convolution [55] to the discrete depth estimation branch. Finally, we employ the deconvolution technique [56] as the bridge between the different branches to balance the feature channels from each branch.

III. APPROACH

Given an input (indoor or outdoor) image \mathbf{I} of size $H \times W$ (H : height and W : width), we aim to predict its depth map $\mathbf{D} \in \mathbb{R}^{H \times W}$ by exploiting the compromise between spatial and depth resolution. The key component of our approach is the proposed *regression-classification cascaded network (RCCN)*. RCCN explicitly models a high spatial resolution discrete depth map \mathbf{D}_1 by discretizing the possible depth interval into a set of discrete values and formulates the estimation of \mathbf{D}_1 as a multi-class classification problem together with the regression of a low spatial resolution continuous depth map \mathbf{D}_0 within the deep architecture. The obtained discrete depth map \mathbf{D}_1 is further refined to obtain a discrete depth map \mathbf{D}_2 in a higher spatial resolution via a refinement network. We describe the detailed architecture of these two networks in Fig. 1 to clearly show their structures and the connections. Last but not least, the depth maps of all three scales (*i.e.*, \mathbf{D}_0 , \mathbf{D}_1 , and \mathbf{D}_2) can be jointly considered within a fusion

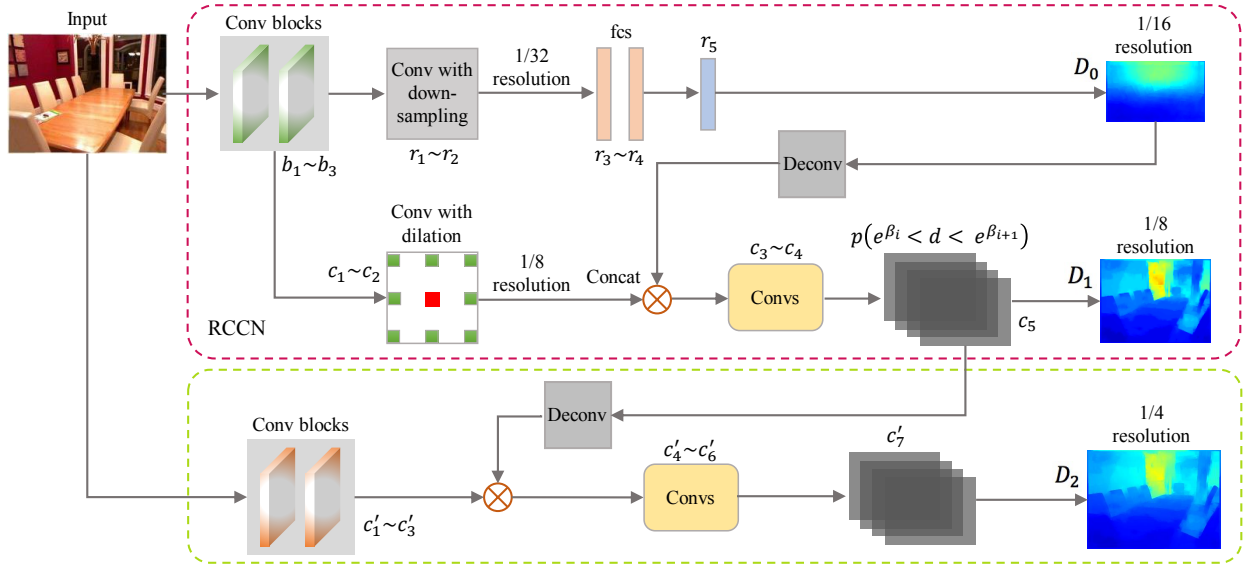


Fig. 1: **Network Architecture** Top: RCCN models the low spatial resolution continuous depth map and the high spatial resolution discrete depth map within a unified network to exploit the compromise between spatial and depth resolution. The regression stage achieves a full-image-view understanding and predicts a low-spatial-resolution continuous depth map. The classification stage takes the low spatial resolution continuous depth map and the convolutional features as inputs, and classifies the pixel at each spatial position to one of the pre-defined discrete depths in a high spatial resolution. Down: The refinement network takes the RGB image and those features from RCCN as inputs, and outputs a discrete depth map in a higher spatial resolution.

network, so as to achieve a continuous depth map \tilde{D}_2^1 . We present the three networks in detail below.²

RCCN	layer	b_1	b_2	b_3	r_1	r_2	r_3	r_4	r_5	De	
	convs	2	2	3	3	3	-	-	-	1	
	chans	64	128	256	512	512	2048	2048	1	512	
	kernel	3	3	3	3	3	-	-	-	4	
	dilat	-	-	-	-	-	-	-	-	-	-
	ratio	/2	/4	/8	16/	32/	-	-	/16	/8	
Refinement	layer	b_1	b_2	b_3	c_1	c_2	Co	c_3	c_4	c_5	De
	convs	2	2	3	3	3	-	1	1	1	1
	chans	64	128	256	512	512	-	2048	2048	M	256
	kernel	3	3	3	3	3	-	3	1	1	4
	dilat	-	-	-	-	2	-	-	-	-	-
	ratio	/2	/4	/8	/8	/8	/8	/8	/8	/8	/8
Refinement	layer	c'_1	c'_2	c'_3			Co	c'_4	c'_5	c'_6	c'_7
	convs	2	2	3			-	1	1	1	1
	chans	64	128	256			-	1024	1024	1024	M
	kernel	3	3	3			-	3	3	1	1
	dilat	-	-	-			-	-	-	-	-
	ratio	/4	/4	/4	/4	/4	/4	/4	/4	/4	/4

TABLE I: **Network Parameters.** Parameters and neurons of the proposed network for NYU Depth V2 dataset based on VGG. b_i : layer shared by the two branches in RCCN. r_i/c_i : layer of the continuous/discrete depth estimation branch. c'_i : layer of the refinement network. Co: concatenation layer. De: deconvolutional layer. M: the number of pre-define sub-intervals.

¹In practice, if the resolution of the depth map output by the deep model is lower than $H \times W$, a classic interpolation method (e.g., linear interpolation) can be used to obtain the depth map at full resolution.

²We introduce our approach based on the network setting for our experiment on NYU Depth V2 dataset and Tab. I provides the associated parameters, so as to facilitate the understanding of the whole approach. The network setting and parameters can be replaced by other appropriate ones.

A. Regression-Classification Cascaded Network

The Regression-Classification Cascaded Network (RCCN) is a joint regressor-classifier. It serves as a two-tier estimator that simultaneously predicts the initial continuous depth map D_0 and the discrete depth map D_1 . We choose to adopt a two-stage cascaded network for modeling and implementing the regression-classification network, aiming to exploit the compromise between low spatial resolution continuous depth and high spatial resolution discrete depth. We also incorporate global scene information from the entire image and structural and contextual information in a large receptive field.

Regressing Continuous Depth: In this stage, the network aims to predict the low spatial resolution continuous depth map D_0 from a global understanding of the entire image, by abstracting a representation feature vector from the whole image field of view. From such a representation, we learn specific non-linear functions for all the pixels located at a pre-defined resolution ($h \times w$).

To this end, on top of the shared convolutional layers (b_1 to b_3), additional convolutional layers (r_1 and r_2) and max-pooling layers with downsampling are used to obtain deeper convolutional features at a coarse resolution. Then, after the pass of two fully-connected (fc) layers (r_3 and r_4), the feature vector will contain high-level information of the whole input image. Followed by a third fc layer (r_5) with $h \times w$ outputs, each output represents the depth value of a spatial location within the pre-defined resolution, and connects to all the vector elements from the last layer, implying a global understanding of the entire image.

This stage is supervised by manually labeled continuous depth values over the whole input image in stride 8 via root

mean squared error in log space (RMSE_{\log}). More specifically, we reshape the hw -dimensional output vector to a $h \times w$ map to obtain the predicted depth map \tilde{D}' at this stage to compare it with the target depth map D' .

It should be noted that, the RMSE_{\log} loss uses a \log function to down-weight the losses in regions with large depth values, which is commonly used as an evaluation metric. From a statistical view, let us consider the generation of data following $y = \exp(\log(x) + N(0, 1))$ with x uniform distributed. It is easy to observe that the noise variance of y is larger when x is larger, implying that the observed depth value has a larger noise variance when its ground truth is larger. Hence, without \log , large depth values would induce an over-strengthened influence on the training process, which is not expected. It also motivates the SID method (instead of uniform quantization) for classification as below, which quantizes depth values with increasing intervals and whose advantage is quantitatively evaluated.

Categorizing Approximate Depth: This stage categorizes each pixel to one of the pre-defined discrete depths in a higher spatial resolution, by taking the shared convolutional features and the previous-stage depth map as inputs.

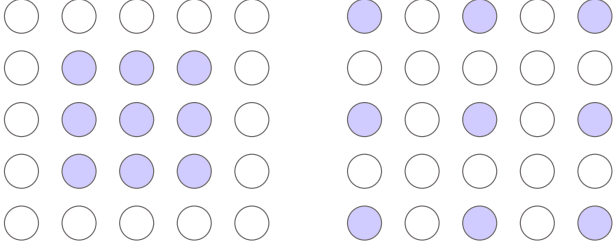


Fig. 2: **Dilated Convolution.** Left: regular convolutional layer (c_1). Right: dilated convolutional layer (c_2).

Specifically, in order to better exploit the compromise between spatial and depth resolution as well as the geometric contexts and physical properties of the image, we adopt a cascaded structure in which the previous-stage depth map is fed into the classification network. The previous-stage depth map is spatially coarse (low spatial resolution) but provides a global-field-of-view understanding of the input image. The shared convolutional features contain finer spatial information. Therefore, on top of the shared convolutional layers, additional convolutional layers (c_1 and c_2) are used to obtain local structural and contextual information. In contrast to the regression branch, we skip the subsampling operation in the max-pooling layers and employ the dilated convolution technique (c_2) [55], which introduces zeros to increase the convolution field to exploit large receptive field information in the fine resolution feature map, as shown in Fig. 2. The predicted continuous depth map is simultaneously deconvoluted to multi-channel feature maps with the same spatial resolution as c_2 . The deconvolution to multi-channel features is an important component to balance the features from different branches. Followed by a concatenation layer, three extra convolutional layers (c_3 to c_5) are applied to learn a richer representation and model the

probabilities of the depth sub-intervals that each pixel belongs to.

This stage is supervised by the pre-defined discrete depths D like semantic labels in segmentation tasks. We minimize the multinomial logistic loss to learn the network parameters.

As for discretization strategies, uniform discretization (UD) is a common way to obtain a set of representative values from a depth interval $[a, b]$. However, considering the facts that the importance of a fixed interval (e.g., $1m$) decreases when the depth ranges from small to large, we propose to use the following spacing-increasing discretization (SID) strategy so that the learned model pays more attention to estimating relatively small depths:

$$\begin{aligned} \text{UD: } l_j &= a + (b - a) * j / K \\ \text{SID: } l_j &= e^{\log(a) + \frac{\log(b/a) * j}{K}} \end{aligned} \quad (1)$$

where K is a pre-define sub-interval number.

B. Learning

Let $\Gamma = \zeta(\Omega, \Upsilon, I)$ denote the feature vector containing m elements outputting from r_4 , where Ω is shared parameters in the *conv* blocks $b_1 \sim b_3$, and Υ is the parameters in $r_1 \sim r_4$. $\Lambda = \xi(\Omega, \Upsilon, \Xi, \Theta_r, I)$ are the feature maps with size $W \times H \times C$ outputting from c_4 , where Ξ is parameters in $c_1 \sim c_4$, and the deconvolutional layer between r_5 and c_3 , Θ_r are parameters of r_5 . $\tilde{D}' = \phi(\Gamma, \Theta)$ of size $W' \times H'$ denotes predicted depth map in the regression stage, and $Y = \psi(\Lambda, \Theta)$ of size $W \times H \times K$ denotes category outputs for each spatial locations, where $\Theta = (\Theta_r; \Theta_c) = (\theta_0, \theta_1, \dots, \theta_{W' * H' - 1}; \theta_{W' * H'}, \dots, \theta_{W' * H' + K - 1})$ are parameters of r_5 and c_5 . The loss function for our RCCN will take the form as:

$$\begin{aligned} \mathcal{L}(\Gamma, \Lambda, \Theta) &= \mathcal{L}_r(\Gamma, \Theta_r) + \mathcal{L}_c(\Lambda, \Theta_c) \\ &= \frac{1}{\mathcal{N}_r} \sum_{w=0}^{W'-1} \sum_{h=0}^{H'-1} \Phi_r(\Gamma, \Theta_r, w, h) \\ &\quad + \frac{1}{\mathcal{N}_c} \sum_{w=0}^{W-1} \sum_{h=0}^{H-1} \Phi_c(\Lambda, \Theta_c, w, h), \quad (2) \\ \Phi_r(\Gamma, \Theta_r, w, h) &= \|\tilde{d}'_{(w,h)} - d'_{(w,h)}\|^2, \\ \Phi_c(\Lambda, \Theta_c, w, h) &= - \sum_{k=0}^{K-1} 1\{d_{(w,h)} = k\} \log(\mathcal{P}_{(w,h)}^k), \\ \mathcal{P}_{(w,h)}^k &= P(\tilde{d}_{(w,h)} = k | \Lambda, \Theta_c), \end{aligned}$$

where $1\{\cdot\}$ is an indicator function, so that $1\{true\} = 1$, and $1\{false\} = 0$, $\mathcal{N}_r = W' \times H'$, $\mathcal{N}_c = W \times H$, $\tilde{d}'_{(w,h)} \in \tilde{D}'$, $d'_{(w,h)} \in D'$, K is the number of sub-intervals, $d_{(w,h)} \in D$ is the ground-truth discrete depth value in spatial location (w, h) . The *softmax* regression for the classification stage computes $\mathcal{P}_{(w,h)}^k$ as:

$$\mathcal{P}_{(w,h)}^k = \frac{e^{y_{(w,h,k)}}}{\sum_{i=0}^{K-1} e^{y_{(w,h,i)}}}, \quad (3)$$

where $y_{(w,h,i)} = \theta_{W' * H' + i}^T \gamma_{(w,h)}$, and $\gamma_{(w,h)} \in \Gamma$.

Method	higher is better			lower is better			
	$\delta < 1.25$	$\delta < 1.25^2$	$\delta < 1.25^3$	Abs Rel	Squa Rel	RMSE	RMSE _{log}
Make3D [3]	0.601	0.820	0.926	0.280	3.012	8.734	0.361
Eigen <i>et al.</i> [51]	0.692	0.899	0.967	0.190	1.515	7.156	0.270
Liu <i>et al.</i> [57]	0.647	0.882	0.961	0.217	1.841	6.986	0.289
LRC (CS + K) [48]	0.861	0.949	0.976	0.114	0.898	4.935	0.206
Kuznietsov <i>et al.</i> [36]	0.862	0.960	0.986	0.113	0.741	4.621	0.189
RCCN-VGG	0.870	0.970	0.993	0.110	0.620	4.029	0.160
RCCN-VGG [†]	0.886	0.975	0.994	0.105	0.540	3.903	0.154
RCCN-ResNet [†]	0.911	0.979	0.993	0.084	0.386	3.072	0.136

TABLE II: **Performance on KITTI test set.** All the scores are evaluated on Eigen *et al.* [51] test split. RCCN-VGG/ResNet: RCCN with backbones of VGG or ResNet. †: RCCN with post refinement processes.

To minimize $\mathcal{L}(\Gamma, \Lambda, \Theta)$, taking derivate with respect to θ_i , $b_1 \sim b_3$ in our experiments³. we can obtain the gradient as:

$$\begin{aligned} \frac{\partial \mathcal{L}(\Gamma, \Lambda, \Theta)}{\partial \theta_i} &= \frac{\partial \mathcal{L}_r(\Gamma, \Theta_r)}{\partial \theta_i} + \frac{\partial \mathcal{L}_c(\Lambda, \Theta_c)}{\partial \theta_i} \\ &= \frac{1}{\mathcal{N}_r} \sum_{w=0}^{W'-1} \sum_{h=0}^{H'-1} \frac{\partial \Phi_r(\Gamma, \Theta_r, w, h)}{\partial \theta_i} \\ &\quad + \frac{1}{\mathcal{N}_c} \sum_{w=0}^{W-1} \sum_{h=0}^{H-1} \frac{\partial \Phi_c(\Lambda, \Theta_c, w, h)}{\partial \theta_i}. \end{aligned} \quad (4)$$

We compute $\frac{\partial \Phi_r(\Gamma, \Theta_r, w, h)}{\partial \theta_i}$ and $\frac{\partial \Phi_c(\Lambda, \Theta_c, w, h)}{\partial \theta_i}$ respectively as follow:

$$\begin{aligned} \frac{\partial \Phi_r(\Gamma, \Theta_r, w, h)}{\partial \theta_i} &= 1\{i < W' * H'\} 1\{i = w * H' + h\} \\ &\quad \times 2(\tilde{d}'_{(w,h)} - d'_{(w,h)})\Gamma, \\ \frac{\partial \Phi_c(\Lambda, \Theta_c, w, h)}{\partial \theta_i} &= 1\{i < W' * H'\} \frac{\partial \Phi_c(\Lambda, \Theta_c, w, h)}{\partial \theta_i} \\ &\quad + 1\{i \geq W' * H'\} \\ &\quad \times \lambda_{(w,h)}(\mathcal{P}_{(w,h)}^i - 1\{\tilde{d}_{(w,h)} = i\}), \end{aligned} \quad (5)$$

where $i \in \{0, 1, \dots, W' * H' + K - 1\}$ and $\frac{\partial \Phi_c(\Lambda, \Theta_c, w, h)}{\partial \theta_i}$ can be computed via chain rules and backpropagation when $i < W' * H'$ (Λ also parameterized by Θ_r).

C. Post Refinement

1) *Refinement network*: By taking the input RGB image and the features of the last classification branches of RCCN as inputs, the refinement network incorporate multi-scale features (implying different receptive field sizes) and refines the discrete depth map into a higher spatial resolution.

Via those convolution blocks (c'_1 to c'_3), we obtain features at a 1/4 resolution of the original image (a relative small receptive field). Similar to the second stage in RCCN, the features (c_5) are deconvoluted into the same resolution of c'_3 with multi-channels outputs. Then, convolutional layers (c'_4 to c'_8) are applied on these two scales of features to obtain the refined discrete depth map. The supervised information in this refinement network is the same as the one in the second stage of RCCN, except for the higher spatial resolution. We initialize the trained parameters of $c'_1 \sim c'_3$ using those of

2) *Fusion Network*: The depth map from the refinement network already incorporates multi-scale features in multi-scale receptive fields, and on average achieves a more accurate depth map estimation than those two predicted maps of RCCN, but not for all individual pixels. There are two possible reasons for such a phenomenon: (i) the refined depth map is still in discrete space; or (ii) depth estimation for some objects (especially for large objects) depends more on information from large receptive fields, and features from small receptive fields may introduce some noises. To address this, we integrate the depth maps from all three scales within the fusion network, which just consists of a few convolutional layers in our experiments. Also, the supervised information in the fusion network is the same as that in the first stage of RCCN except for the higher spatial resolution.

IV. EXPERIMENTS

To validate the compromise principle and demonstrate the effectiveness of RCCN, here we present a number of experiments examining different aspects of the approach. After introducing the common experimental settings, we evaluate our methods on three challenging datasets, *i.e.* *NYU Depth V2* [1], *KITTI* [2], and *Make3D* [30], [3], via the error metrics using in previous works.

A. Experimental Setting

1) *Implementation Details*: In order to fairly compare the proposed method with the current state-of-the-art methods, our method adopts both VGG-16 [62] and ResNet-101 [63] as our backbone. We initialise the parameters of RCCN in base convolutional layers via the pre-trained classification model on ILSVRC [64]. The training procedures for RCCN-VGG and RCCN-ResNet are a little different. For RCCN-VGG, we directly train our network follows a polynomial decay with a base learning rate of 0.0001, the power of 0.9, the momentum of 0.9, and the weight decay of 0.0005. However, for RCCN-ResNet, we find that directly optimize our network with a large base learning rate resulting an unexpected divergence after some iterations, and a small base learning

³Note that $c'_1 \sim c'_3$ are independent from $b_1 \sim b_3$.

	R	C	RRCN	RCCN	CCCN	D_0	RCCN- D_0
$\delta < 1.25$	0.732	0.806	0.762	0.852	0.835	0.741	0.750
$\delta < 1.25^2$	0.905	0.947	0.928	0.963	0.950	0.913	0.919
$\delta < 1.25^3$	0.951	0.985	0.968	0.990	0.982	0.956	0.960
Abs Rel	0.172	0.142	0.162	0.123	0.132	0.168	0.162
Squa Rel	1.105	0.892	1.060	0.763	0.893	1.092	1.071
RMSE	5.829	4.711	5.105	4.235	5.102	5.476	5.265
RMSE _{log}	0.282	0.198	0.235	0.174	0.208	0.270	0.247

TABLE III: **Variants of RCCN on KITTI dataset.** R: Directly learning continuous depth in a fine scale via regression. C: Directly learning discrete depth in a fine scale via classification with proposed SID strategy. RRCN: Learning continuous depth via a cascaded regression-regression structure. RCCN: The proposed method. CCCN: A classification-classification cascade network. Note that, higher is better in top table, while lower is better in bottom table.

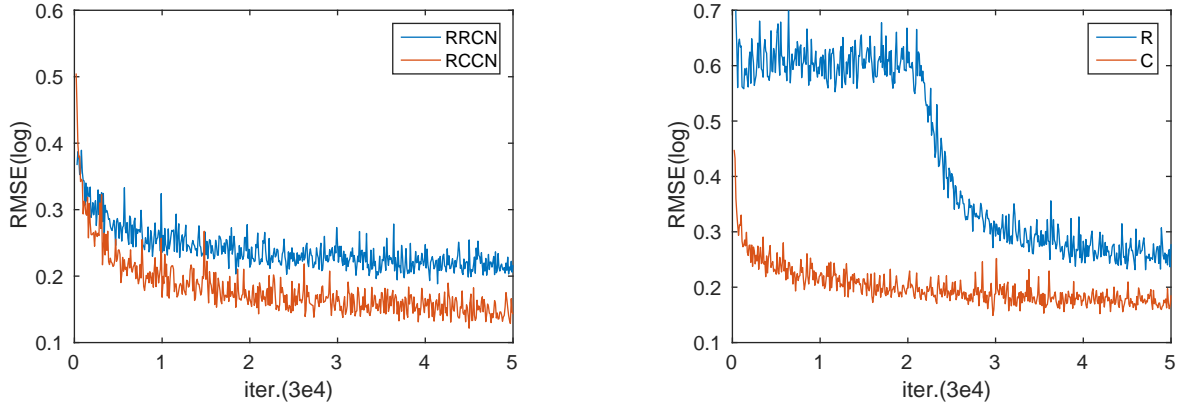


Fig. 3: **Training Error on KITTI dataset.** Left: Training errors of RCCN and RRCN. Right: Training error of R and C. From the two illustrations, our classification strategy (C) for depth estimation can make the neural network converge to a better solution rather than regression strategy (R).

rate resulting slow convergence rate. To speed up training, we fixed all the parameters in the base convolutional layers, and first train the regression stage for a few iterations, and then train the two stage for some other iterations with a base learning rate of 0.001. And finally, we optimize all the parameters together in RCCN-ResNet with a base learning rate of 0.0001. Further, the networks in post refinement stages are independently trained with fixed parameters of RCCN. The proposed method is implemented via a public deep learning platform *Caffe* [65], and trained on 4 TITAN X GPUs with 12GB of memory per GPU with batch size of 4.

2) *Data Augmentation*: Following previous works [51], [52], we employ some data augmentation techniques to prevent overfitting and to learn a better model in the training process, including: (i) *Random Cropping*: we randomly crop rectangles with predefined sizes from the original image. (ii) *Flipping*: we randomly flip the original image horizontally. (iii) *Scaling*: we randomly resize the original image by a scale factor belongs to the interval of $[0.75, 1.25]$, and normalize the associated depth map with the corresponding scales. (iv) *Rotation*: we randomly rotate the input image with the degree of $[-10^\circ, 10^\circ]$.

3) *Evaluation Metrics*: Below are the list of depth error metrics based on which the quantitative evaluation is per-

formed:

$$\begin{aligned}
 \text{Accuracy} &: \frac{1}{T} \sum_{i \in T} 1\{\delta = \max(\frac{d_i}{\hat{d}_i}, \frac{\hat{d}_i}{d_i}) < thr\} \\
 \text{Abs Rel} &: \frac{1}{N} \sum_{i \in N} \frac{|d_i - d_i^*|}{d_i^*} \\
 \text{Squa Rel} &: \frac{1}{N} \sum_{i \in N} \frac{\|d_i - d_i^*\|^2}{d_i^*} \\
 \text{RMSE} &: \sqrt{\frac{1}{N} \sum_{i \in N} \|d_i - d_i^*\|^2} \\
 \text{RMSE}_{log} &: \sqrt{\frac{1}{N} \sum_{i \in N} \|\log(d_i) - \log(d_i^*)\|^2} \\
 \text{Ave log}_{10} &: \frac{1}{N} \sum_{i \in N} |\log_{10}(d_i) - \log_{10}(d_i^*)|
 \end{aligned} \tag{6}$$

B. KITTI

The KITTI dataset [2] contains some outdoor scenes captured by cameras and depth sensors in a driving car. All the 61 scenes from the “city”, “residential”, and “road” categories consist of our training/test sets. We test on 697 images from 29 scenes split by [51], and train on 23,486 images from the remaining 32 scenes. All the images are resize to a

Method	higher is better			lower is better			
	$\delta < 1.25$	$\delta < 1.25^2$	$\delta < 1.25^3$	Abs Rel	Squa Rel	RMSE	RMSE _{log}
Make3D [3]	0.447	0.745	0.897	0.349	0.492	1.214	0.409
DepthTransfer [18]	0.460	0.742	0.893	0.350	0.539	1.1	0.378
Liu <i>et al.</i> [40]	0.475	0.770	0.911	0.335	0.442	1.06	0.362
Ladicky <i>et al.</i> [21]	0.542	0.829	0.941	-	-	-	-
Li <i>et al.</i> [58]	0.621	0.886	0.968	0.232	-	0.821	-
Wang <i>et al.</i> [32]	0.605	0.890	0.970	0.220	0.210	0.745	0.262
Roy <i>et al.</i> [33]	-	-	-	0.187	-	0.744	-
Liu <i>et al.</i> [57]	0.650	0.906	0.976	0.213	-	0.759	-
Eigen <i>et al.</i> [34]	0.769	0.950	0.988	0.158	0.121	0.641	0.214
Chakrabarti <i>et al.</i> [59]	0.806	0.958	0.987	0.149	0.118	0.620	0.205
Laina <i>et al.</i> [52]	0.629	0.889	0.971	0.194	-	0.790	-
Xu <i>et al.</i> [60]	0.636	0.896	0.972	0.193	-	0.792	-
Li <i>et al.</i> [61]	0.789	0.955	0.988	0.152	-	0.611	-
Laina <i>et al.</i> [52] [†]	0.811	0.953	0.988	0.127	-	0.573	0.195
Li <i>et al.</i> [61] [†]	0.788	0.958	0.991	0.143	-	0.635	-
Xu <i>et al.</i> [60] [†]	0.811	0.954	0.987	0.121	-	0.586	-
RCCN-VGG	0.753	0.937	0.983	0.165	0.138	0.607	0.213
RCCN-VGG [†]	0.765	0.950	0.991	0.160	0.131	0.586	0.204
RCCN-ResNet [†]	0.807	0.957	0.992	0.136	0.116	0.564	0.199

TABLE IV: **Performance on NYU Depth v2 test set.** All the scores are evaluated on official test split. RCCN-VGG/ResNet: RCCN with backbones of VGG or ResNet. †: RCCN with post refinement processes.

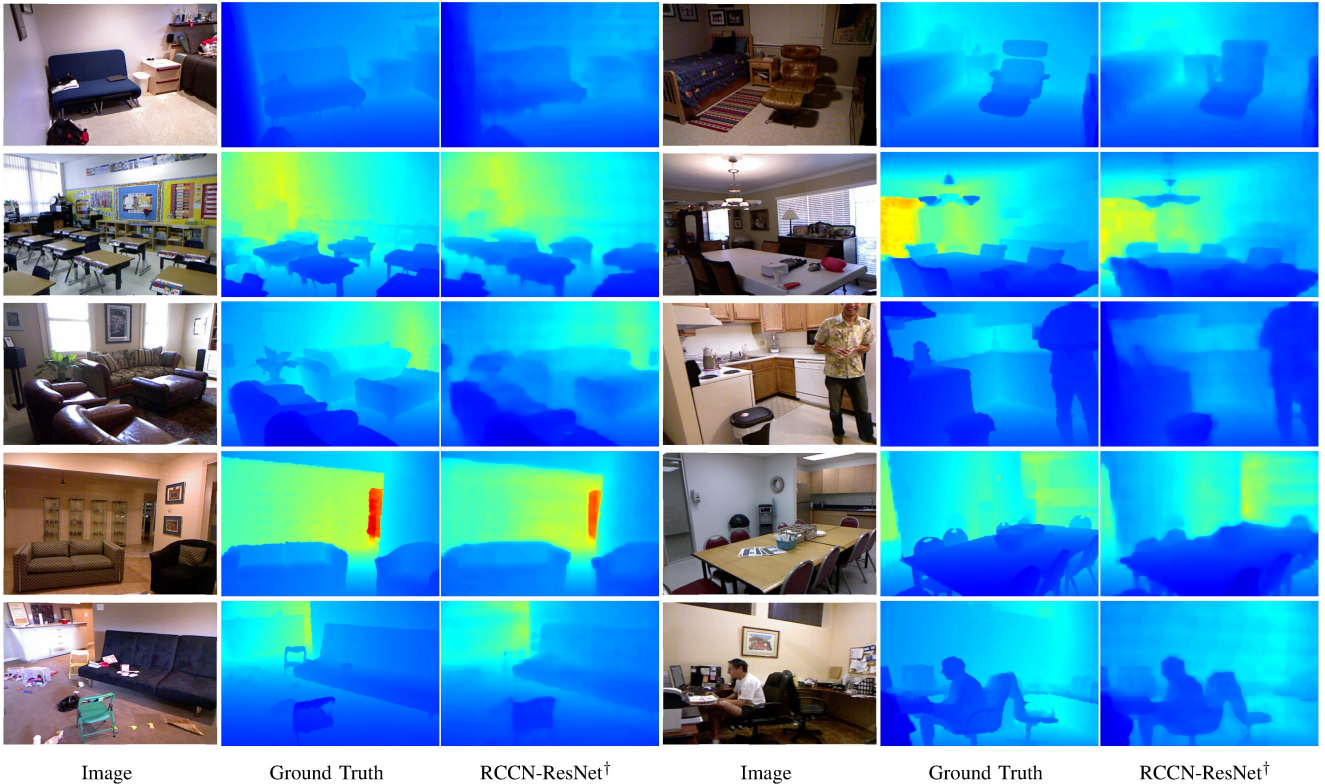


Fig. 4: **Depth Prediction on NYU Depth v2.**

resolution of 385×769 from 375×1241 . We train our model on a random crop of size 385×385 . At the test time, we split each image to 3 overlapping windows and obtain the predicted depth values in overlapped regions by averaging the 3 predictions. The evaluation metrics are computed on a pre-

defined center cropping by Eigen *et al.* [51] in the original resolution. Note that, since the ground truth depth are provided for only about 15% of points within the bottom part of the image, some depth targets in the bottom parts are filled using the colorization routine in the NYU Depth development kit

Algorithm	C1 error			C2 error		
	Abs Rel	Ave \log_{10}	RMSE	Abs Rel	Ave \log_{10}	RMSE
Make3D [3]	-	-	-	0.370	0.187	-
Liu <i>et al.</i> [66]	-	-	-	0.379	0.148	-
DepthTransfer [18]	0.355	0.127	9.20	0.361	0.148	15.10
Liu <i>et al.</i> [40]	0.335	0.137	9.49	0.338	0.134	12.60
Li <i>et al.</i> [58]	0.278	0.092	7.12	0.279	0.102	10.27
Liu <i>et al.</i> [57]	0.287	0.109	7.36	0.287	0.122	14.09
Roy <i>et al.</i> [33]	-	-	-	0.260	0.119	12.40
Laina <i>et al.</i> [52]	0.176	0.072	4.46	-	-	-
LRC-Deep3D [49]	1.000	2.527	19.11	-	-	-
LRC [48]	0.443	0.156	11.513	-	-	-
Kuznietsov <i>et al.</i> [36]	0.421	0.190	8.24	-	-	-
Xu <i>et al.</i> [60]	0.184	0.065	4.38	0.198	4.53	8.56
RCCN-VGG [†]	0.252	0.104	8.82	0.255	0.106	11.57
RCCN-ResNet [†]	0.189	0.082	5.57	0.192	0.088	9.34

TABLE V: Performance on Make3D test set. LRC-Deep3D [49] is adopting LRC [48] on Deep3D model [49].

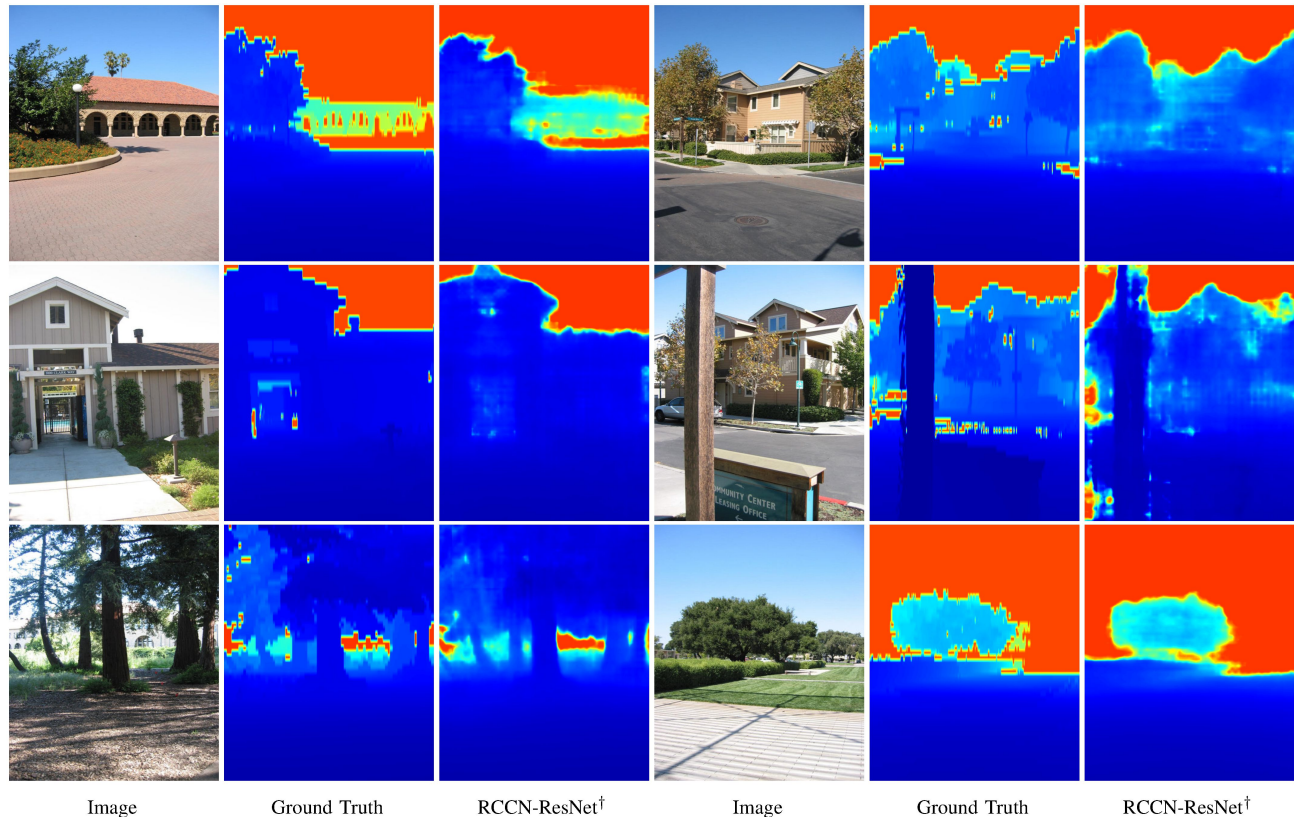


Fig. 5: Depth Prediction on Make3D test set.

[67] for our training images following [51].

Besides those representative quantitative results shown in Fig. 6, we summarize the quantitative evaluation in Tab. II, which demonstrates that the proposed approach significantly outperforms those previous methods in all those considered error metrics.

To further exploit the compromise principle and demonstrate the effectiveness of the proposed RCCN, we learn some related network variants by directly regressing continuous depth, directly estimating discrete depth via classification, jointly

modeling continuous depth via our network architecture, and learning a classification-classification cascade network. From the quantitative results shown in Tab. III and Fig. 3, we can conclude that: 1) when treating depth estimation as a classification problem instead of regression, the network can converge to a better local solution on average; 2) image-receptive-field-of-view understanding, as well as local high-level convolutional features indeed help deep networks better learn the depth distribution of a scene; 3) the compromise between spatial and depth resolutions simplifies network train-

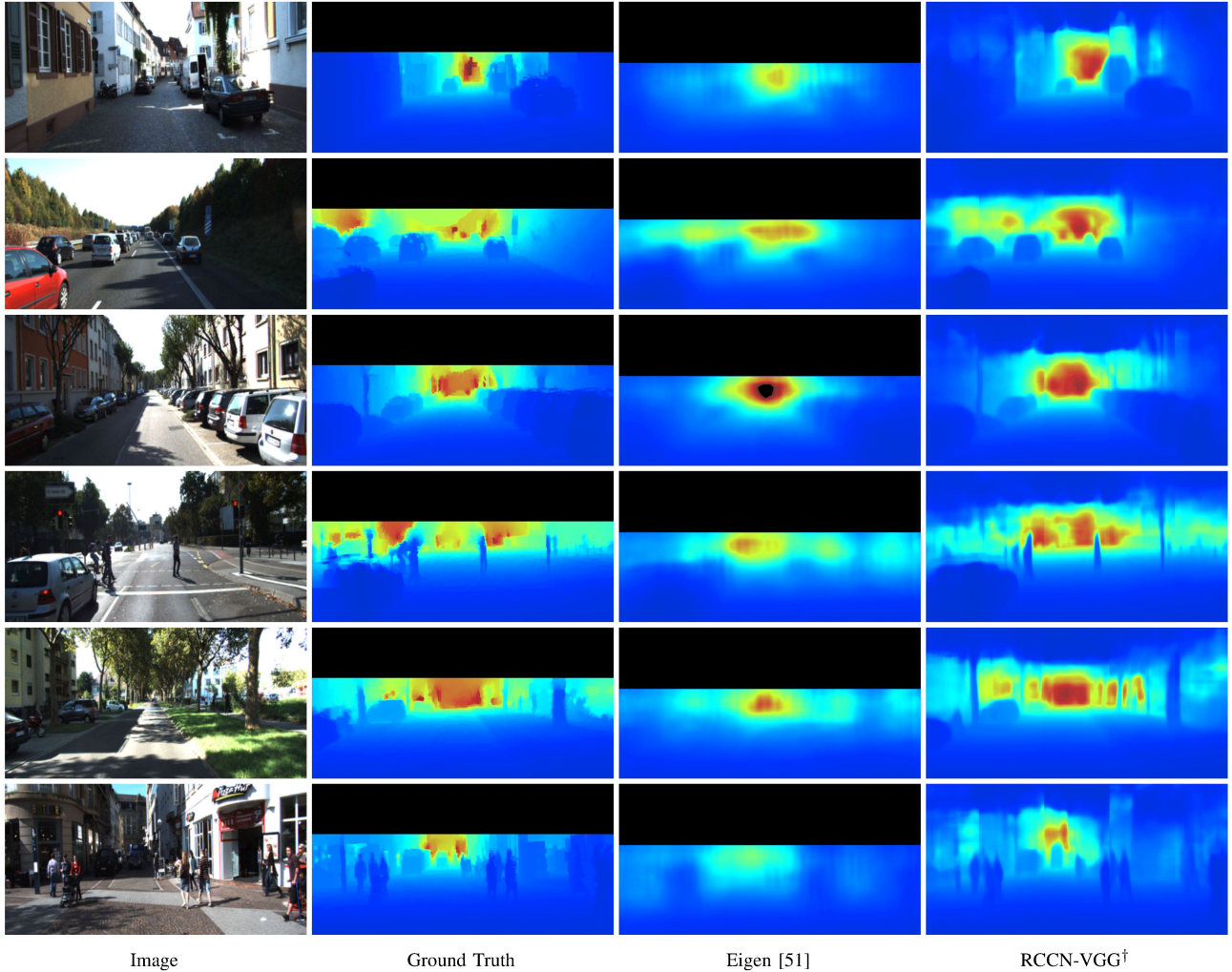


Fig. 6: **Depth Prediction on KITTI test set.** The depth values in the black parts are not provided by KITTI.

ing; 4) The performances of RRCN and of RCCN deteriorate once removing the low-spatial resolution branch D_0 from them (leading to R, C, respectively), demonstrating that D_0 benefits D_1 ; 5) The comparison between D_0 and RCCN- D_0 shows that D_1 also benefits D_0 ; and 6) From the observation that $\text{RCCN} > \text{CCCN} > \text{RRCN}$, It can be seen that high spatial resolution together with high depth resolution leads to worse results.

C. NYU Depth V2

The NYU Depth V2 [1] contains 464 indoor video scenes taken with a Microsoft Kinect camera. We randomly sample half of the 120K images from the raw dataset according to the official split training scenes as our training sets, and test on the 694-image test set. We train our model on a randomly crop of size 240×320 . On top of those qualitative results in Fig. 4, we report in Tab. IV the quantitative results via several common metrics used in previous works [34], [31]. The predictions from our model yields comparable or state-of-the-art results comparison with previous works. Specifically, the estimated coarse continuous depth outperforms the “Coarse+Fine” prediction of Eigen *et al.* [51]. The predicted

high spatial resolution discrete depth in particular obtains an impressive improvement, demonstrating that both discrete depth and the proposed RCCN framework are effective.

D. Make3D

The Make3D dataset [30], [3] contains 534 outdoor images, 400 for training, and 134 for testing, with the resolution of 2272×1704 . Our model is trained on a random crop of size 480×320 . In the test phase, we split the test images into some 480×320 sub-images, and use max pooling on the overlapping regions to obtain the final predictions. As shown in Tab. V, we report $C1$ and $C2$ error on this dataset [18]. We achieve state-of-the-art performance in all error metrics.

E. Generalization to Cityscapes

We also demonstrate the generalization ability of our model. Specifically, we test our model trained only on KITTI via images provided by Cityscapes [68], which is also a large benchmark for auto-driving. As shown in Fig. 7, our KITTI model can capture the general scene layout and objects such as cars, trees and pedestrians much well in images from Cityscapes.

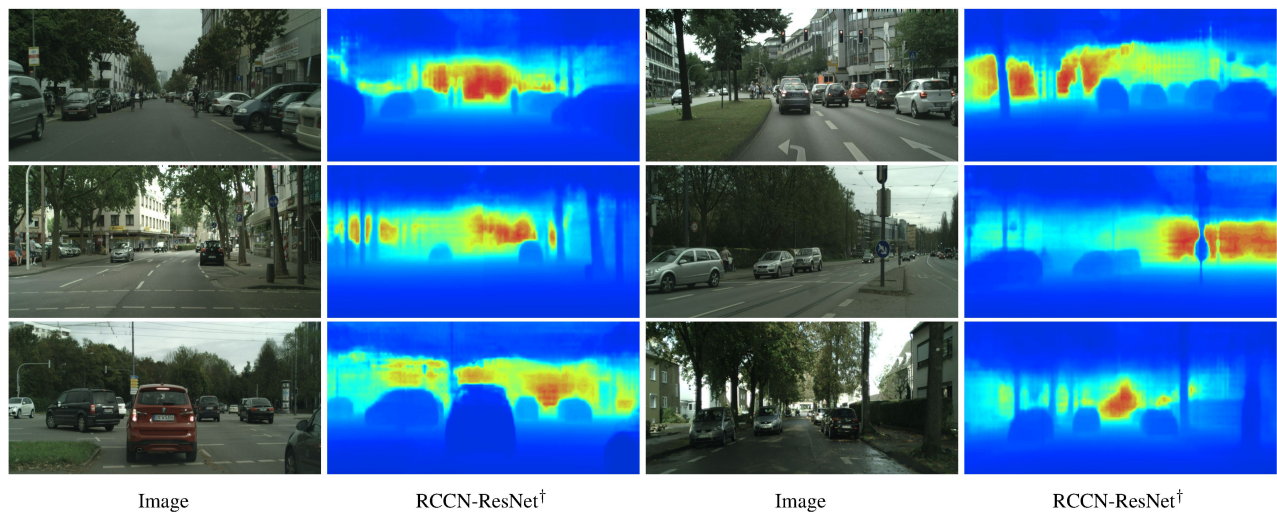


Fig. 7: **Generalization to Cityscapes.** The model is trained only on KITTI, and test on Cityscapes.

V. CONCLUSION

In this paper, we have presented a deep CNN architecture for MDE. Based on the fact that training a network to estimate a high spatial resolution continuous depth map is difficult, we hypothesize to design network architectures according to the compromise principle that training a network to estimate a depth map with reduced spatial resolution or depth resolution is easier. According to the compromise principle, we propose a regression-classification cascaded network to jointly model continuous depth and discrete depths in two branches. The proposed approach is validated on three widely-used and challenging datasets, where it achieves competitive or state-of-the-art results. Moreover, specific experiments have been done and the obtained results demonstrate that our network is superior to its variants, which also validates the design of our approach to some extent. We will continue to investigate new methodologies to reduce the depth resolution and extend our framework to other challenging dense prediction problems.

REFERENCES

- [1] P. K. Nathan Silberman, Derek Hoiem and R. Fergus, "Indoor segmentation and support inference from rgb-d images," in *ECCV*, 2012.
- [2] A. Geiger, P. Lenz, C. Stiller, and R. Urtasun, "Vision meets robotics: The kitti dataset," *IJRR*, 2013.
- [3] A. Saxena, M. Sun, and A. Y. Ng, "Make3d: Learning 3d scene structure from a single still image," *IEEE TPAMI*, vol. 31, no. 5, pp. 824–840, 2009.
- [4] L. Sheng, J. Cai, T.-J. Cham, V. Pavlovic, and K. N. Ngan, "A generative model for depth-based robust 3d facial pose tracking," *CVPR*, 2017.
- [5] S. Savarese and L. Fei-Fei, "3d generic object categorization, localization and pose estimation," in *ICCV*, 2007.
- [6] D. Sun, E. B. Sudderth, and M. J. Black, "Layered image motion with explicit occlusions, temporal consistency, and depth ordering," in *NIPS*, 2010.
- [7] D. Hoiem, A. A. Efros, and M. Hebert, "Automatic photo pop-up," *ACM TOG*, vol. 24, no. 3, pp. 577–584, 2005.
- [8] W. Sun, G. Cheung, P. A. Chou, D. Florencio, C. Zhang, and O. C. Au, "Rate-constrained 3d surface estimation from noise-corrupted multiview depth videos," *IEEE TIP*, vol. 23, no. 7, pp. 3138–3151, 2014.
- [9] K. Müller, H. Schwarz, D. Marpe, C. Bartnik, S. Bosse, H. Brust, T. Hinz, H. Lakshman, P. Merkle, F. H. Rhee *et al.*, "3d high-efficiency video coding for multi-view video and depth data," *IEEE TIP*, vol. 22, no. 9, pp. 3366–3378, 2013.
- [10] T.-Y. Chung, J.-Y. Sim, and C.-S. Kim, "Bit-allocation algorithm with novel view synthesis distortion model for multiview video plus depth coding," *IEEE TIP*, vol. 23, no. 8, pp. 3254–3267, 2014.
- [11] S. Hou, Z. Wang, and F. Wu, "Deeply exploit depth information for object detection," in *CVPRW*, 2016.
- [12] M. Kiechle, S. Hawe, and M. Kleinsteuber, "A joint intensity and depth co-sparse analysis model for depth map super-resolution," in *CVPR*.
- [13] H. Ha, S. Im, J. Park, H.-G. Jeon, and I. S. Kweon, "High-quality depth from uncalibrated stereo motion clip," in *CVPR*, 2016.
- [14] N. Kong and M. J. Black, "Intrinsic depth: Improving depth transfer with intrinsic images," in *ICCV*, 2015.
- [15] Y. Liu, X. Cao, Q. Dai, and W. Xu, "Continuous depth estimation for multi-view stereo," in *CVPR*, 2016.
- [16] M. Poostchi, H. Aliakbarpour, R. Viguier, F. Bunyak, K. Palaniappan, and G. Seetharaman, "Semantic depth map fusion for moving vehicle detection in aerial video," in *CVPRW*.
- [17] B. Li, L.-Y. Duan, C.-W. Lin, T. Huang, and W. Gao, "Depth-preserving warping for stereo image retargeting," *IEEE TIP*, vol. 24, no. 9, pp. 2811–2826, 2015.
- [18] K. Karsch, C. Liu, and S. B. Kang, "Depth transfer: Depth extraction from video using non-parametric sampling," *IEEE TPAMI*, vol. 36, no. 11, pp. 2144–2158, 2014.
- [19] A. Rajagopalan, S. Chaudhuri, and U. Mudenagudi, "Depth estimation and image restoration using defocused stereo pairs," *IEEE TPAMI*, vol. 26, no. 11, pp. 1521–1525, 2004.
- [20] D. Hoiem, A. A. Efros, and M. Hebert, "Recovering surface layout from an image," *IJCV*, vol. 75, no. 1, pp. 151–172, 2007.
- [21] L. Ladicky, J. Shi, and M. Pollefeys, "Pulling things out of perspective," in *CVPR*, 2014.
- [22] J. Konrad, M. Wang, and P. Ishwar, "2d-to-3d image conversion by learning depth from examples," in *CVPRW*, 2012.
- [23] A. A. Alatan and L. Onural, "Estimation of depth fields suitable for video compression based on 3-d structure and motion of objects," *IEEE TIP*, vol. 7, no. 6, pp. 904–908, 1998.
- [24] R. Lai, Y. Shi, K. Scheibel, S. Fears, R. Woods, A. W. Toga, and T. F. Chan, "Metric-induced optimal embedding for intrinsic 3d shape analysis," in *CVPR*, 2010.
- [25] Z. Yang, Z. Xiong, Y. Zhang, J. Wang, and F. Wu, "Depth acquisition from density modulated binary patterns," in *CVPR*, 2013.
- [26] I. Tomic and K. Berkner, "Light field scale-depth space transform for dense depth estimation," in *CVPRW*, 2014.
- [27] J. Lin, X. Ji, W. Xu, and Q. Dai, "Absolute depth estimation from a single defocused image," *IEEE TIP*, vol. 22, no. 11, pp. 4545–4550, 2013.
- [28] W. Dong, G. Shi, X. Li, K. Peng, J. Wu, and Z. Guo, "Color-guided depth recovery via joint local structural and nonlocal low-rank regularization," *IEEE TMM*, vol. 19, pp. 293–301, 2017.
- [29] H. Sheng, S. Zhang, X. Cao, Y. Fang, and Z. Xiong, "Geometric occlusion analysis in depth estimation using integral guided filter for light-field image," *IEEE TIP*, vol. 26, pp. 5758–5771, 2017.

- [30] A. Saxena, S. H. Chung, and A. Y. Ng, "Learning depth from single monocular images," in *NIPS*, 2006.
- [31] F. Liu, C. Shen, and G. Lin, "Deep convolutional neural fields for depth estimation from a single image," in *CVPR*, 2015.
- [32] P. Wang, X. Shen, Z. Lin, S. Cohen, B. Price, and A. Yuille, "Towards unified depth and semantic prediction from a single image," in *CVPR*, 2015.
- [33] A. Roy and S. Todorovic, "Monocular depth estimation using neural regression forest," in *CVPR*, 2016.
- [34] D. Eigen and R. Fergus, "Predicting depth, surface normals and semantic labels with a common multi-scale convolutional architecture," in *ICCV*, 2015.
- [35] S. Kim, K. Park, K. Sohn, and S. Lin, "Unified depth prediction and intrinsic image decomposition from a single image via joint convolutional neural fields," in *ECCV*, 2016.
- [36] Y. Kuznetsov, J. Stückler, and B. Leibe, "Semi-supervised deep learning for monocular depth map prediction," *CVPR*, 2017.
- [37] D. Scharstein and R. Szeliski, "A taxonomy and evaluation of dense two-frame stereo correspondence algorithms," *IJCV*, vol. 47, no. 1-3, pp. 7-42, 2002.
- [38] D. Forsyth and J. Ponce, *Computer Vision: a Modern Approach*. Prentice Hall, 2002.
- [39] W. Zhuo, M. Salzmann, X. He, and M. Liu, "Indoor scene structure analysis for single image depth estimation," in *CVPR*, 2015.
- [40] M. Liu, M. Salzmann, and X. He, "Discrete-continuous depth estimation from a single image," in *CVPR*, 2014.
- [41] A. Oliva and A. Torralba, "Modeling the shape of the scene: A holistic representation of the spatial envelope," *IJCV*, vol. 42, no. 3, pp. 145-175, 2001.
- [42] C. Liu, J. Yuen, and A. Torralba, "Sift flow: Dense correspondence across scenes and its applications," *IEEE TPAMI*, vol. 33, no. 5, pp. 978-994, 2011.
- [43] J. Dai, K. He, and J. Sun, "Instance-aware semantic segmentation via multi-task network cascades," in *CVPR*, 2016.
- [44] C. Szegedy, S. Ioffe, and V. Vanhoucke, "Inception-v4, inception-resnet and the impact of residual connections on learning," *arXiv preprint arXiv:1602.07261*, 2016.
- [45] Y. Sun, X. Wang, and X. Tang, "Deep convolutional network cascade for facial point detection," in *CVPR*, 2013.
- [46] G.-J. Qi, "Hierarchically gated deep networks for semantic segmentation," in *CVPR*, 2016.
- [47] R. Garg, G. Carneiro, and I. Reid, "Unsupervised cnn for single view depth estimation: Geometry to the rescue," in *ECCV*, 2016.
- [48] C. Godard, O. Mac Aodha, and G. J. Brostow, "Unsupervised monocular depth estimation with left-right consistency," *CVPR*, 2017.
- [49] J. Xie, R. Girshick, and A. Farhadi, "Deep3d: Fully automatic 2d-to-3d video conversion with deep convolutional neural networks," in *ECCV*, 2016.
- [50] X. Wang, D. Fouhey, and A. Gupta, "Designing deep networks for surface normal estimation," in *CVPR*, 2015.
- [51] D. Eigen, C. Puhrsch, and R. Fergus, "Depth map prediction from a single image using a multi-scale deep network," in *NIPS*, 2014.
- [52] I. Laina, C. Rupprecht, V. Belagiannis, F. Tombari, and N. Navab, "Deeper depth prediction with fully convolutional residual networks," in *3DV*, 2016.
- [53] D. Zoran, P. Isola, D. Krishnan, and W. T. Freeman, "Learning ordinal relationships for mid-level vision," in *ICCV*, 2015.
- [54] W. Chen, Z. Fu, D. Yang, and J. Deng, "Single-image depth perception in the wild," in *NIPS*, 2016.
- [55] L.-C. Chen, G. Papandreou, I. Kokkinos, K. Murphy, and A. L. Yuille, "Deeplab: Semantic image segmentation with deep convolutional nets, atrous convolution, and fully connected crfs," *arXiv:1606.00915*, 2016.
- [56] M. D. Zeiler, D. Krishnan, G. W. Taylor, and R. Fergus, "Deconvolutional networks," in *CVPR*, 2010.
- [57] F. Liu, C. Shen, G. Lin, and I. Reid, "Learning depth from single monocular images using deep convolutional neural fields," *IEEE TPAMI*, vol. 38, no. 10, pp. 2024-2039, 2016.
- [58] B. Li, C. Shen, Y. Dai, A. van den Hengel, and M. He, "Depth and surface normal estimation from monocular images using regression on deep features and hierarchical crfs," in *CVPR*, 2015.
- [59] A. Chakrabarti, J. Shao, and G. Shakhnarovich, "Depth from a single image by harmonizing overcomplete local network predictions," in *NIPS*, 2016.
- [60] D. Xu, E. Ricci, W. Ouyang, X. Wang, and N. Sebe, "Multi-scale continuous crfs as sequential deep networks for monocular depth estimation," *CVPR*, 2017.
- [61] J. Li, R. Klein, and A. Yao, "A two-streamed network for estimating fine-scaled depth maps from single rgb images," in *ICCV*, 2017.
- [62] K. Simonyan and A. Zisserman, "Very deep convolutional networks for large-scale image recognition," in *ICLR*, 2015.
- [63] K. He, X. Zhang, S. Ren, and J. Sun, "Deep residual learning for image recognition," in *CVPR*, 2016.
- [64] O. Russakovsky, J. Deng, H. Su, J. Krause, S. Satheesh, S. Ma, Z. Huang, A. Karpathy, A. Khosla, M. Bernstein, A. C. Berg, and L. Fei-Fei, "ImageNet Large Scale Visual Recognition Challenge," *IJCV*, vol. 115, no. 3, pp. 211-252, 2015.
- [65] Y. Jia, E. Shelhamer, J. Donahue, S. Karayev, J. Long, R. Girshick, S. Guadarrama, and T. Darrell, "Caffe: Convolutional architecture for fast feature embedding," *arXiv preprint arXiv:1408.5093*, 2014.
- [66] B. Liu, S. Gould, and D. Koller, "Single image depth estimation from predicted semantic labels," in *CVPR*, 2010.
- [67] A. Levin, D. Lischinski, and Y. Weiss, "Colorization using optimization," *ACM TOG*, vol. 23, no. 3, pp. 689-694, 2004.
- [68] M. Cordts, M. Omran, S. Ramos, T. Rehfeld, M. Enzweiler, R. Benenson, U. Franke, S. Roth, and B. Schiele, "The cityscapes dataset for semantic urban scene understanding," in *CVPR*, 2016.